Published in final edited form as:
*Comput Biol Med*. 2011 December ; 41(12): 1100–1109. doi:10.1016/j.compbiomed.2011.07.008.

# Anatomic and electro-physiologic connectivity of the language system: a combined DTI-CCEP study

**Christopher R Conner**, **Timothy Ellmore**, **Michael A DiSano**, **Thomas A Pieters**, **Andrew Potter**, and **Nitin Tandon**
Vivian Smith Department of Neurosurgery University of Texas Medical School at Houston

## Abstract

Here we present a novel multimodal analysis of network connectivity in the language system. We assessed connectivity of Broca's area using tractography with diffusion tensor imaging (DTI), and with cortico-cortical evoked potentials (CCEPs) that measure the spread of artificial currents applied directly to cortex. We found that both the amplitude and latency of CCEP currents significantly correlates ($r^2 = 0.41$, $p<10^{-16}$) with the number of DTI pathways connecting the stimulation and recording loci. This strategy of relating electrical information flow with the neural architecture will likely yield new insights into cognitive processes.

### Keywords

Cortico-cortical evoked potentials; diffusion-weighted MRI; Broca's area; connectivity; epilepsy; intracranial stimulation; language; phonation; articulation; arcuate fasciculus

## Introduction

A major endeavor of systems neuroscience is to understand how the various components of brain networks are interconnected [1, 2]. Cerebral connectivity cannot be measured directly in humans with techniques such as invasive tract tracing, [3] and is derived indirectly using techniques such as resting state measures [4-6] or task weighted fMRI connectivity [7, 8]. A recent advance in assessing cerebral connectivity is the application of diffusion tensor imaging (DTI) tractography to identify pathways in the brain. DTI tractography provides information about anatomic white matter connectivity between brain regions, but not about the directionality of these connections. Additionally, tractography methods are subject to processing steps that include the use of arbitrary thresholds to quantify the integrity of particular pathways [9]. The thresholds for ascribing significance to a particular pathway, and the components of diffusion weighted imaging that should be used to establish connectivity, is a topic of ongoing research. This issue is of particular importance in a disseminated system such as that involved in language comprehension and production. In this work we sought to relate tractography data to an electro-physiologic measure of



Address Correspondence to: Nitin Tandon UT Houston Medical School 6431 Fannin St. Suite G.500 Houston, TX 77030 nitin.tandon@uth.tmc.edu Phone: (713) 500-5475 Fax: (713) 500-0723.



**Conflicts of Interest:** None Declared

connectivity that is task independent and relies on artificial electrical stimulation using brief current pulses.

Our goal was to determine the relationship between connectivity assessed using DTI pathway density with data evaluated from the spread of artificially applied electrical currents to the brain. This was accomplished using intracranial electrodes and the mapping of cortico-cortical evoked potentials (CCEPs) [10-13]. CCEPs offer the advantage of measuring structural connectivity in vivo between brain regions, with less ambiguity than neuroimaging. Unlike task dependent measures of functional connectivity such as MEG [14, 15], fMRI [16-18], or PET [19], CCEPs provide paradigm independent maps of connectivity that present a more holistic and unbiased estimate of cortical connectivity. The generation of this CCEP response has been attributed to orthodromic responses induced by stimulation that originate in neurons residing in layer III [10]. Prior CCEP studies [10, 12] have also estimated the velocity of information flow between regions where CCEPs are evoked, and have sought to link them to the directness of the connection between these regions and to the velocity of conduction of information between them. When the evoked potential of the CCEP is broken down by amplitude and latency, it can be used to investigate the speed and bandwidth of signal propagation via the white matter tracts. Such information is complimentary to DTI tractography. Despite multiple advances in DTI methods, only one effort at correlating CCEPs with tractography [20] has ever been attempted, and to the best of our knowledge, there are no publications in the peer reviewed literature that compare connectivity using these two methods.

For the comparison of CCEPs and DTI we choose the language system as our model network because of its dense connectivity between spatially distribution regions. Broca's area (BA) has also been of great interest to the cognitive neuroscience community, given its diverse roles in varieties of language processes, especially in semantic and phonologic processes. Due to its importance, it has been assessed using diverse strategies including lesional analyses [21, 22], functional imaging [23-25] and DTI [26-28]. While only a handful of publications have applied CCEPs to the evaluation of human cerebral connectivity, the first and most widely known of these studies, deals with electro-physiologic connectivity of BA to Wernicke's area [10]. For all of these reasons, we chose BA as the first region to for the systematic evaluation of DTI and CCEP estimates of connectivity.

The combination of tractography and task independent electrophysiology will provide insight into the interpretation of DTI data. Regions that are functionally connected to the stimulation site may display varied CCEP responses based on the nature of the connection (multi-synaptic, cortico-sub-cortico-cortical connection, excitatory or inhibitory etc.). In this manner, CCEP connectivity can be expected to reveal all regions that lie under one of the subdural electrodes (SDEs) and receive inputs from the stimulated region. DTI connectivity, however, is likely to yield only direct connectivity information. Taken together, the comparison of anatomical (DTI) connectivity with CCEPs can be used to determine the electro-physiological correlates of DTI-determined connectivity. This comparison can also be used to determine the appropriate thresholds that should be applied to DTI datasets in order to imply that a connection has a high likelihood of supporting the transmission of meaningful amounts of information. We hypothesize that white matter fiber tract density correlates directly with the amplitude and inversely with speed of current spread between the cortical regions connected by specific white matter tracts. We specifically predict that this relationship will manifest as a positive correlation between density, defined as the number of pathways comprising the tracts connecting BA with distal regions, and the amplitude and the latency of the earliest deflection seen on the CCEP recording on distal electrodes following stimulation of BA. These hypotheses are also consistent with the predictions of cable theory

[29], which implies that more densely packed or more heavily myelinated axons comprising fiber bundles identified by tractography would mediate a greater and faster flow of information.

## Methods

Seven patients (5 female, mean age 36.8 +/- 16.0 years) with pharmacologically resistant epilepsy, who were scheduled for left hemispheric subdural electrode [30] implantation to localize the seizure onset site, were enrolled in the study (Table 1). Informed consent was obtained following study approval by our institution's committee for protection of human subjects. Five of the seven patients underwent a Wada test [31] to identify the language dominant hemisphere, and in all cases language was lateralized to the left hemisphere.

### MR Data Acquisition

Prior to surgery, imaging was carried out on a 3T whole-body MR scanner (Philips Medical Systems, Bothell WA) equipped with a 16-channel SENSE head coil. Anatomical images were collected using a magnetization-prepared 180 degree radio-frequency pulses and rapid gradient-echo (MP-RAGE) sequence, optimized for gray-white matter contrast, with 1 mm thick sagittal slices and an in-plane resolution of 0.938 × 0.938 mm. Diffusion weighted images were collected with the Philips 32-direction diffusion encoding scheme (high angular resolution), with the gradient overplus option along with a b0 (non-diffusion-weighted) image volume. Seventy axial slices were acquired with a 224 × 224 FOV (2mm slice thickness, 1.75 × 1.75 mm pixels) and a maximum b-value of 800 s $mm^{-2}$.

### Image Analysis

Anatomical image realignment, spatial normalization transformation, and tensor calculations were performed in AFNI [32]. The T1 anatomical MRI for each subject was used to construct mesh models of the gray/white matter interface and pial surface using FreeSurfer v4.5 [33, 34]. Surface reconstructions were visualized in Matlab v7.7.0 (Mathworks, Natick MA) using custom software. For each subject the diffusion weighted volumes and gradient table were realigned to the skull-stripped anatomical MR volume. A single-model diffusion tensor was computed using these realigned volumes. A flowchart of the complete processing stream is provided in Figure 1. Details of the diffusion imaging acquisition parameters and deterministic DTI tractography generation are available in prior publications, and also in the companion paper by Tertel et al in this issue [35, 36].

### Electrode Localization

Following electrode implantation, a high-resolution contiguous thin-slice CT scan was acquired (0.5 mm in-plane resolution, 1 mm thick axial slices). This CT scan was co-registered to the pre-operative anatomical MR imaging using a rigid-body transformation algorithm implementing a mutual information cost function [32]. The centers of individual electrodes were localized using the post-operative CT and then transformed to the image space of the anatomical MR. A non-linear deformation of the cortical surface, and hence the locations of the SDEs, occurred following electrode implant. To correct for these deformations, the pial cortical surface model was modified, disregarding fissures and sulci, to create a smoothed envelope that exactly fits the shape and size of the subject's brain. SDEs were realigned to this new surface by displacing them along a surface normal to the point on the envelope closest to their location on the deformed brain surface. Intra-operative photographs taken at the time of SDE removal were used to make final adjustments to the SDE locations determined by this automated method. SDEs could then be visualized as spherical geometric objects on cortical surface model in SUMA [37] or Matlab. Details of these methods were previously published [38, 39]. Using FreeSurfer (v4.5) [40], the SUMA

surface was automatically parcellated and the electrodes that overlay pars opercularis (PO) or pars triangularis (PT) of BA were identified.

We have previously shown [36, 41] that the automatic anatomically parcellation scheme, applied here to delineate Brodmann areas 44 and 45, yields a very precise and reliable estimate of the anterior termination of the arcuate fasciculus and of language sites localized in Broca's area. Therefore, we applied this automated localization algorithm as the strategy to determine which electrodes to stimulate during CCEP measurement. Given that CSM carries a small risk of seizure induction, it was performed on purely clinical grounds, with other electrodes chosen for CCEP stimulation based on the automated gyral parcellation scheme (Table 1). In addition to the grouped analysis for all BA electrodes, we also analyzed the data from these two localization methods separately (Figure 6).

## Cortical Stimulation Mapping

Mapping of language cortex for clinical purposes was performed using visual stimuli (Boston Naming Test) [42], auditory repetition, and naming of common objects using auditory stimuli [43, 44]. In some cases, this included mapping of the electrodes identified as lying over BA (PO or PT). Tasks were performed during constant current stimulation of adjacent pairs of electrodes with a Grass Stimulator (Grass Technologies, West Warwick, RI USA). Cortical stimulation mapping (CSM) was carried out with 3-5s 50 Hz trains, alternating polarity square-wave pulses (0.3 ms) with intensity varying from a minimum of 2 mA to a maximum of 10 mA, in steps of 2 mA. During stimulation the patient was monitored for after discharges, motor dysfunction, or sensations due to stimulation of somato-sensory cortex. CSM sites were considered as positive for language if stimulation caused articulation arrest, dynosmia, or anomia [36, 44].

## Cortico-Cortical Evoked Potentials

Electrodes overlying BA, as identified by the FreeSurfer parcellation map or by CSM, were targeted for measuring CCEPs. These electrode pairs were stimulated with bipolar pulses (10 mA, 500 ms total, 250 ms up/down, at 1 Hz for 50 seconds) with the Grass Stimulator. Concurrent electro-corticography (ECoG) was collected at 1 kHz on the remaining SDEs using NeuroFax (Nihon Kohden). Channels were initially referenced to an artificial 0 V, and inspected for stimulus artifact or spike activity. A subgroup of all of the electrodes (>20) with minimal noise, stimulus artifact, and evoked potentials were used to generate an average reference for all electrodes.

ECoG data collected during stimulation at each pair of electrodes over BA were exported to Matlab (bandwidth – 0.2 to 300 Hz), and epochs were time locked at the beginning of each stimulus. Noisy trials containing inter-ictal epileptiform discharges or artifacts were also identified at this point and excluded from further analysis. There were >45 epochs for each stimulating pair. A high pass filter ($10^{th}$ order Chebyshev, 1 Hz cutoff, 30 dB side lobe attenuation) was applied to each channel to minimize the effects of voltage drift. Epochs were averaged together to obtain the CCEP at each recording electrode.

Positive and negative deflections in the averaged CCEP response at each electrode were identified using an automated peak detection algorithm (in-house software). Data within the first 8 ms were excluded to eliminate the stimulation artifacts. An approximation to the first derivative was used to find local minima and maxima used for feature extraction. The first clear negative deflection following the stimulus artifact was defined as an N1 response [10, 11] (Figure 2). Only negative deflections within 40 ms of stimulus artifact were classified as N1 responses in order to minimize the influence of indirect connections not present in the

tractography. Channels with N1 peaks of amplitude >1000 mV were excluded, as they likely reflected non-biological electrical transmission.

### Tractography

Deterministic tractography was performed in DTIQuery v1.1 [45] using the streamline tracking technique (STT) [46] with 2.0 mm seed point spacing, 2.0 mm path step size, and maximum path length 300 mm. By aligning the anatomical MR to the DTI images, fiber pathways stayed in their native imaging space and could be localized in relation to the cortical surface. Tractography data were saved as a pathway database file and imported into Matlab as the set of all pathways present in the subject's brain. Virtual cuboidal VOIs of size 20×20×20mm were placed around each electrode, and all pathways passing through this VOI were selected. Overlap of pathways passing from one VOI to another could then be quickly calculated and saved for further analysis. For each stimulating pair, the number of pathways passing through the VOI surrounding either electrode was included (logic OR function). The number of pathways passing from this first waypoint to each of the other recording electrodes was calculated and saved (logic AND function).

### Co-representation of CCEPs and DTI

The tractography and CCEPs for each stimulation pair were co-represented in Matlab with a semi-transparent model of the left hemisphere (Figure 3). SDEs were depicted as spheres on the cortical surface, with stimulating electrodes shaded black for graphical representation and recording electrodes colored and scaled based on the N1 response. Recording electrodes without an N1 were shown in white. All pathways passing through the cuboidal VOIs around the stimulation pair have been drawn as green streamlines. These pathways were not constrained by the location of the SDEs, and represent all the fiber tracts passing near the stimulating electrodes.

### Correlation

For each stimulating pair, the N1 amplitudes and corresponding latencies at each channel were collated with the number of pathways connecting the stimulating pair to those electrode locations, and then imported into R (R Foundation for Statistical Computing v2.11.1) for statistical analysis. Electrodes without an identifiable N1 response were excluded. All data for the 10 stimulating pairs were pooled together for the correlation analysis. Amplitude and latency were regressed against number of tracts to determine the effect of path density on evoked potential. The regression equation was:

$$P_i=\beta_o+\beta_a A_i+\beta_l L_i+\epsilon$$

where $P_i$ was the number of pathways connecting the stimulating pair to the $i^{th}$ electrode, $A_i$ the amplitude of the CCEP, $\beta_a$ the coefficient of the amplitude, $L_i$ the latency, $\beta_l$ the latency coefficient, $\beta_o$ the intercept and the error term $\varepsilon$.

### Grouped analysis of CCEP data

Given the variability in the coverage provided by the SDEs, we wanted to be able to visualize the CCEP response across all individuals concurrently to make summary statements for the CCEP responses seen for the group. For this purpose, we transformed the locations of all SDEs used for ECoG and stimulation to a standard anatomy – the Montreal Neurologic Institute imaging space (Colin N27 brain), using a 12 parameter affine transformation. The electrodes were then represented on the pial surface of this brain generated in SUMA. This surface was visualized as a 3D object in Matlab, as previously described, and individual electrodes were assigned distinct colors based on amplitude of the

N1 response. Electrodes without an N1 response were left uncolored (white). Next, a spatial map of the probability of the presence of a CCEP response was computed. Each node on the cortical surface was assigned a proportional value - the ratio of the number of electrodes within 7 mm that showed a CCEP response >10 μV to the numbers of electrodes present within 7 mm. The distance of 7 mm as the length that a subdural macroelectrode records from was arrived at based on recent ECoG analysis in this lab that is currently the subject of another publication which is in review.

## Application

Our seven subjects had 837 implanted SDEs, and a total of 10 stimulation pairs that lay over BA and were used for stimulation (Table 1). Five patients had a single pair of stimulating electrodes over BA. The remaining two patients, no. 4 and 6, had multiple pairs of stimulating electrodes over BA. In six of the ten stimulation pairs, both the electrodes lay over PT, in three both were over PO, and in the last instance one electrode was in each of the two sub-regions. The final data set included 1248 electrodes where ECoG was carried out during stimulation and used for the CCEP computation. Of these, an overt N1 CCEP response was recorded from 404 electrodes. The average amplitude for these responses was 103.0 +/- 157 μV and the mean latency was 23.3 +/- 7.8 ms. Stimulation at each pair was considered independent from the others, even if two pairs were stimulated in the same subject, as they related to distinct tractography pathways. CCEPs at the recording electrodes were considered for each stimulation pair individually, meaning that some electrodes were included up to three times (as in subject no. 4).

Across all subjects we noted low latency, high amplitude responses over pars orbitalis, sensorimotor mouth/face motor cortex, lateral premotor cortex and middle frontal gyrus (dorso-lateral prefrontal cortex). These N1 responses were >100 mV in amplitude with very brief delays (15-20 ms). In keeping with the strong short-range inter-areal connectivity of the human cortex, the largest amplitude responses with the shortest latencies were noted at electrodes immediately adjoining the stimulation pair. The DTI tractography paths connecting BA to these areas consisted of large, cortico-cortical U fiber pathways (Figure 3). These short-range connections were the densest of all fiber tracts originating or terminating in BA. For electrodes that showed an N1 response, and which were situated within 2 cm of the stimulating pair (n = 74), i.e. in the adjoining gyrii, there were an average of 245 +/- 174 (range 10 to 908) fiber paths connecting them with the stimulating pair. The average fractional anisotropy (FA) along these fibers was 0.39 +/- 0.03 and their mean length was 55.9 +/- 14.8 mm. CCEPs measured at these electrodes had average N1 peak of 285.8 +/- 260.0 μV and a latency of 18.7 +/- 5.5 ms.

Relatively distant components of the language system also showed clear CCEP responses in most cases. They were notable over posterior middle temporal gyrus (MTG), posterior superior temporal gryus (STG) (both corresponding to Wernicke's area), inferior parietal lobule and parts of the anterior STG and MTG. For electrodes beyond 2 cm of the stimulating pair with an N1 response and at least one fiber connecting them to the stimulating pair (n = 135), there were an average of 28 +/- 38 fibers (range 1 to 202) in the path. The average FA along these fibers was 0.41 +/- 0.06 and the mean length was 78.6 +/- 33.4 mm. CCEPs measured at these electrodes had an average N1 peak of 78.1 +/- 95.3 μV and a latency of 23.8 +/- 7.6 ms. Some electrodes situated over the anterior STG demonstrated both the high amplitude, low latency and the smaller, slower N1 responses of posterior STG. In six of the seven patients, tracts connecting the BA stimulating electrodes to these distant language sites were also noted (Figure 3). These pathways terminated variably over the posterior MTG and STG, the inferior parietal lobule and the anterior STG.

Overall, the comparison of connectivity between these two modalities showed remarkable co-localization of the CCEPs and the tracts for electrodes both proximate and remote to the stimulation pair. Both DTI and CCEPs revealed an anterior to posterior connection that coincided well with the anatomical location of the arcuate fasciculus (AF) and was consistent with our prior findings that relate CSM sites to the AF [36]. To quantify the relationship between these two measures of connectivity, the amplitude and latency of all N1 responses were correlated with the number of tracts connecting the stimulating pair with each recording electrode (Figure 4). Amplitude of the N1 response correlated positively with increasing path size ($\beta_a = 0.45$, $p < 2\times10^{-16}$), indicating that higher magnitude responses were related to denser pathways connecting the regions near the electrodes. On the other hand, latency correlated negatively ($\beta_l = -2.63$, $p = 1\times10^{-5}$) with numbers of tracts, possibly indicating that smaller, less dense tracts mediated slower signal transmission. The overall $r^2$ for the regression considering both of these variables was 0.41 ($p < 2.2\times10^{-16}$, $F_{2,401} = 140.3$). Co-linearity or dependence of N1 amplitude with latency was explored by fitting a linear regression between these two variables. The $r^2$ for this relationship was 0.01, and while statistically significant ($p < 0.01$), is not biologically meaningful and is not considered further. Additionally, a linear regression using both latency and amplitude along with an interaction term between them was computed. The F statistic for this model was 111.7 (df = 3, 404) and the $r^2$ was 0.45. An ANOVA between the original model and this one does show that the expanded model (the model including the interaction term) is statistically better than the original ($p < 3\times10^{-8}$). However, the AIC for the two models are very similar, 4804 for the model in the paper and 4775 the expanded model. We therefore feel that including an interaction term is not necessary because it is not a meaningful improvement over the first model.

In the analysis reported here, we included only electrodes where N1 evoked potentials were noted after stimulation. When we repeated the same analysis including all of the electrodes, similar relationships between the N1 (amplitude and latency), and the DTI data were noted. The amplitude of the N1 response positively correlated ($\beta_a = 0.48$, $p < 2\times10^{-16}$) and latency was negatively correlated ($\beta_l = -0.91$, $p = 1.3\times10^{-5}$). As expected, given the larger numbers of data points closer to the origin, the $r^2$ for this dataset was 0.25, nevertheless, the model was still very significant ($F = 209$, df = 2, 1222, $p < 2\times10^{-16}$).

An important issue is the effect of distance of the recording electrodes from the stimulating pair. This could affect both the amplitude and latency of the CCEP response. It therefore is important to evaluate such an effect to determine the specificity of tractography in estimating the electro-physiologic connectivity. This would make certain that our analysis is exploiting additional data from the tractography rather a decay in evoked current strength and an increase in latency that are distance dependent distance. To examine this we computed a regression of the CCEP amplitude and latency against this distance. This model was first run using only electrodes with an N1 response and resulted in an $r^2$ of 0.25, which compares with the $r^2$ of 0.41 when DTI was used in the regression. When all electrodes were considered, these numbers were 0.13 and 0.25, respectively.

The grouped display of the CCEP responses (Figure 5a), for all seven individuals, corroborated and more clearly defined the connectivity pattern across individuals. Identification of sites where effects were noted was based on standard localization strategies used to report activation sites in functional imaging. Sites where CCEPs were localized in standardized space (Talairach co-ordinates), using localization tools in AFNI are reported. In some cases additional confirmation of localization was also obtained by performing CSM. Large responses were noted in the frontal cortex adjoining BA, including the premotor cortex (PMC) (known to be involved in articulation) [47], the face motor cortex, parts of the middle frontal gyrus involved in working memory (dorso-lateral prefrontal cortex – DLPFC)

and PO. The lower amplitude CCEPs were present in the inferior parietal lobe, the posterior STG and MTG (Wernicke's area), and along the anterior STG and MTG. In four of the patients (1, 2, 5, 7) stimulation over posterior MTG/STG resulted in receptive language deficits. In the other cases (3, 4, 6), Wernicke's area was identified anatomically as the posterior and inferior portion of Brodmann Area 22 in the remaining subjects. The population probability map (Figure 5b) allowed for an interpretation of the CCEP data that was unbiased by the amplitude, and that allowed for interaction of data collected across all the individuals. A highlight of this analysis is the distinct and robust response noted over the posterior MTG, and the adjoining STG coinciding with the location of Wernicke's area. Other robust CCEP responses were over PO, PMC, DLPFC, M1 face, and the anterior temporal lobe (STG and MTG).

The results of the CSM have been summarized in Figure 6. All CSM data were collected at a fixed stimulation current that was maximized based on the presence of focal after discharges and the absence of evoked responses (motor phenomena, phosphenes, pain) [44]. As noted in the methods, we selected electrodes for CCEPs based on their location over BA. Some of these electrodes were also positive for CSM, others were negative for CSM, and at some, CSM was not performed, as it was not relevant for clinical purposes (Table 1). We also performed subgroup analyses of CCEP estimates of connectivity for electrode pairs over BA that were positive for CSM and those that were negative for CSM. These results were vastly similar though differed due to variations in cortical coverage in these two groups (Figure 6).

## Discussion

This is the first effort to relate anatomic and task-free electrophysiological measures of connectivity in the human brain. It proves the feasibility and the utility of multimodal assessments of connectivity in the language system. This study confirms findings in the prior literature that describe connections of BA using CCEPs [10] and DTI [26, 48] as independent estimators of connectivity. BA connects very strongly with other parts of prefrontal and premotor cortex, pars orbitalis, face motor cortex, Wernicke's area, anterior temporal lobe and the inferior parietal lobule (Figures 3,5). CCEPs occurring within 40 ms of stimulation explain approximately 41% of the variance in connectivity defined by tractography (Figure 4). This estimate incorporates only two features of the CCEP response at each electrode: the latency and amplitude of the N1 evoked potential. Slower or subsequent peaks in the evoked potential are not considered. These variables were regressed against a simple measure of DTI connectivity: the number of tracts in the fiber pathway. Using even these relatively simple metrics derived of the electro-physiologic and imaging data, our study demonstrates a high degree of correlation between them. Furthermore, these results suggest that CCEPs can offer information beyond the scope of the network architecture estimated using only DTI, extending to provide information about the capacity and speed of signal transmission. A recent report by Keller et al showed that a measure of functional connectivity, resting state fMRI (rsfMRI), correlates well with CCEP recordings. In their findings, the authors used the N2 response to quantify the level of connectivity, although they note that other evoked potentials (N1 or P1) yielded similar results. They found that the magnitude of the N2 response correlated with rsfMRI connectivity, and reached the conclusion that the strongest functional connections relate to the strongest electrical connections [49]. Our work is in keeping with their results, as well as other prior observations suggesting that combinations of DTI data with other modalities like fMRI [41] and CSM [36] provide unique insights into cerebral connectivity.

Work by Matsumoto [10] revealed latencies of about 30 ms for CCEPs recorded over specific posterior language sites following BA stimulation. We found that CCEPs in posterior sites also occurred in the same time range. In our analysis we restricted the CCEP

responses to those that occurred within 40 ms to isolate those that resulted from direct/monosynaptic connections [10, 53]. Beyond this time window other responses were noted and likely resulted from subcortical and indirect (multi-synapse) connections (Figure 2). For the vast majority of electrodes analyzed in this study, the N1 potential was the first and only potential identified. This is in keeping with prior CCEP reports [12]. In addition, the negative (N1) response suggests that the evoked potential has a distribution consistent with a focal cortical depolarization. The choice to use the N1 response was based on the literature where this potential had a distribution over regions thought to be connected to the area of CCEP stimulation [10, 54]. Because this analytic method relates two measures that have previously not been correlated, we chose a system (the language network) and a measure (the N1 potential) that both have replicable findings. Given DTI method used here was limited to direct connections, it was necessary to bias our CCEP measures in the same fashion. The exploration of indirect connections using CCEPs and DTI in tandem will be expanded in further studies. Such indirect pathways also provide important routes for information flow and may be crucial for recovery from insults to the arcuate fasciculus that occur following strokes, tumor growth, and other brain insults.

The differences in latencies and amplitudes between distinct CCEP responses suggest connections that vary in number or quality. The negative correlation between latency and the number of fiber paths confirmed this conjecture (Figure 4). Lower quality fiber bundles had fewer tracts identified by deterministic tractography and longer latencies with lower peak amplitudes. The amplitude of the N1 response had a strong, positive correlation with fiber number. However, both latency and amplitude of the CCEP response might be affected by metrics of path quality other than numbers of fibers (e.g. mean FA along the path). To examine this relationship thoroughly, we compared electrodes within 2 cm of the stimulating pair and found abundant fiber paths (mean number = 245) with high mean FA (0.39) that was significantly lower ($p=0.001$) than more remote electrodes (mean FA = 0.41, mean number = 28). Further, the latency (18.7 vs. 23.8 ms) and the peak amplitude (285.6 μV vs. 78.1 μV) relating to these two sets were distinctly different ($p<10^{-7}$ and $p<10^{-8}$ respectively). Thus, longer range CCEPs appear to be mediated by longer fibers, which may also necessarily have greater values for their mean anisotropy. Other metrics such as radial and axial diffusivity [73, 74] also impact path quality and will be explored further in later analyses. The integration of DTI path measures with CCEP responses (albeit in a patient population) is likely to provide insights into which parameters of the DTI are meaningful in regards to information flow. This would allow for an objective means of evaluating DTI measures as they apply to various disease states [9], and to the study of connectivity in non-patient populations, where intracranial electrophysiology data are sparse or impossible to collect.

As we note in the results, there is very weak correlation between the two measures of the CCEP response – amplitude and latency. While this may initially appear counter-intuitive, on closer evaluation, it is not so. The window of time used to isolate the N1 response was 40 ms. This might allow for some indirect connections between the stimulation and recording sites. Signal amplitude modulation is likely to occur at these intermediate sites, uncoupling the relationship between amplitude and latency of the CCEP response. Additionally, latency measures are subject to a lower bound, below which signal transmission is physiologically impossible. At proximate sites though, amplitude of the response is not subject to these bounds.

A greater understanding of cortico-cortical information flow is essential for system neuroscientists to construct more ecologically valid representations of network connectivity in the brain [63, 64]. Stimulation based methods (CCEPs, TMS) are truly “task-independent” and uninfluenced by task-based recruitment of individual regions. It is

possible that stimulation based connectivity estimates may lead to some antidromic information flow. However, the majority of the networks revealed by them are likely to relate to orthodromic connections that are dependent upon the obligate connectivity of the region being assessed. Prior studies combining stimulation with neuroimaging have included comparisons of concurrent TMS-PET [19, 55-58], TMS-fMRI [59] or TMS-event-related scalp potentials [53]. TMS stimulation preferentially causes sulcal activation [60] and its effects are hard to accurately model or predict [61]. Additionally, TMS of some brain regions that are overlaid by temporalis muscle can be painful. Other areas, such as the basal temporal region, cannot be targeted because they are located very deep relative to where the TMS coil is placed. All of these factors limit the utility of this non-invasive stimulating technique. Stimulation using implanted electrodes suffers from none of these limitations. It is remarkably spatially specific, and local current spreads can be modeled reasonably [62]. Its major limitation is that the method can only be applied to a patient population. Analyzing data across multiple patients with varied etiology and sites of seizure onset allowed us to project our connectivity findings to a normal population. The connectivity maps from CCEPs can be considered the obligatory connectivity of the stimulated region.

In addition to stimulation based techniques, there is available repertoire of ‘relatively’ task unbiased estimates of connectivity using neuroimaging. These include rsfMRI [65, 66], meta-analyses of functional imaging data sets [67, 68], and tractography [69-71]. While rsFMRI provides estimates of task free connectivity, it cannot completely overcome the confounds of activity in the default mode network [72]. Other Imaging based tractographic measures outline pathways, but provide no information about the valence or the functional relevance of synaptic connections subserved by these tracts. Meta-analytic connectivity maps draw upon data acquired over a wide range of tasks to minimize the influence of a single task on the connectivity estimates. But though they may reveal the scope of regional connectivity engaged by task performance, they do not reflect the “hard wired” connections of a given region in the manner most unequivocally illustrated by stimulation-based mapping techniques.

Our method of correlating electrophysiology and imaging relies on accurate localization of SDEs after implantation. DTI connections are very sensitive to location, and large errors could significantly shift the VOIs around the electrodes, thus degrading the correlation. We have shown previously [35, 36] that the semi-automated method of electrode localization used here allows for the appropriate comparisons between these data sets. The fact that we found anticipated connections of the AF with typical language sites further validates our electrode localization scheme.

We used BA as the subject of this inter-modal integrative connectivity analysis as this is a region of intense interest to cognitive neuroscience. BA also has dense connectivity with local and remote areas that has been anticipated by prior anatomic and lesional analyses, and allows for a robust comparison of connectivity measures [21, 22, 50]. One of the most prominent fiber tracts leaving, the AF, has been shown to be a brain pathway in which several fibers have some of the highest FA values in the brain [41, 51, 52]. Connectivity estimates of BA using tractography overlap well with anatomical dissections of the white matter tracts involved in language [26-28]. However, while DTI has been very useful in supporting existing models of language generation [48], it has not generated new insights into the operations of this region that is crucial to language. The combination of electro-physiologic connectivity with anatomic pathways is likely to yield such insights.

As revealed by the correlation measures, the overlap between the two connectivity estimates is not perfect. This may partially be a consequence of inaccuracies in both measures. During CCEPs, we assume that the cortical region producing the evoked response lies directly

below the electrode measuring it. This is obviously an oversimplification, and is likely to result in inaccuracies as the tracts used in the correlation are based on the location of the electrode and not the source of the signal. Additionally, we have only correlated the DTI data with the N1 response [10, 54]. It is certainly possible that some direct connections are mediated by very slow fibers or by multiple intra-cortical synapses that lead to slower information flow than we expect to see. In distinction to the prior work focusing on the N1 [10, 54] or N2 [49], future work will relate DTI measures to more complex estimates of the mean evoked response.

Deterministic tractography has known problems with fiber tracing at the terminations of pathways in gray matter [75]. VOIs at the cortical surface are prone to inaccuracies in counting the number of fiber pathways reaching them; one result being lower pathway numbers than expected given a certain CCEP response. Despite this, we found excellent correlation between the DTI tractography and the evoked potentials: DTI fiber numbers can reveal information about the ability of a fiber pathway to transmit electrical signals. This analysis serves to validate deterministic analysis of DTI data, showing that “stronger” pathways are more capable of transmitting high amplitude signals at faster rates. Further work could provide preliminary estimates for the quality of pathway necessary to act as a conduit in a network. An expansion on this could lead to a more objective method for thresholding and constraining DTI results in subjects that do not have invasive electrophysiology. This work can also be expanded to compare inter-areal connectivity using probabilistic tractographic techniques [75] with CCEPs.

## Summary

Our work describes a novel method for correlating two task independent connectivity estimates – DTI tractography and cortico-cortical evoked potentials (CCEPs) – in a patient population. We evaluated the language system, as its connectivity profile is relatively well understood and it is comprised of both short and long-range connections. CCEPs were recorded from a broad set of cortical regions during low frequency stimulation of subdural electrodes placed over BA. DTI tractography was constrained to pathways passing through VOIs centered at stimulation electrodes at each of the recording electrodes. This allowed for a direct comparison of connectivity between the two modalities. To test the hypothesis that two components of the CCEP response were predictive of DTI connectivity density, the amplitude and latency of the N1 evoked potential were regressed against the number of fiber pathways terminating in the regions around the stimulating and recording electrodes. The results of the regression demonstrated a significant correlation between the two modalities with CCEPs explaining approximately 41% of the variance in DTI tractography. Evoked responses were noted over canonical language sites in prefrontal cortex as well as the inferior parietal lobule and in both the anterior and posterior lateral temporal cortex. The distribution of these responses coincided well with the termination of white matter fiber tracts passing near the stimulating electrode pairs in BA. The methodology here outlines a regression analysis that is flexible enough to use any quantifiable DTI or CCEP results. It is therefore possible to use other measures of pathway strength, even non-deterministic DTI processing algorithms. Such alternatives could include measures of pathway integrity (fractional anisotropy, mean diffusivity), or they could employ probabilistic tractography [75] to determine connectivity.

## Acknowledgments

We would like to thank Vips Patel for his help with MR scanning, the nurses and the EEG technicians at the epilepsy monitoring unit at Memorial Hermann Hospital for facilitating patient recordings, Jeremy Slater, Giridhar Kalamangalam and Omotola Hope for contributing patients to the study, and Stephen Dreyer for initial programming of electrode localization software. NT is supported by a K12 grant from the National Institutes of

Health Clinical and Translational Award KL2 RR0224149 and by the Vivian Smith Foundation for Neurologic Research. TME is partially supported by the Epilepsy Foundation.

## References


1. Crick F, Koch C. Constraints on cortical and thalamic projections: the no-strong-loops hypothesis. Nature. 1998; 391:245–250. [PubMed: 9440687]
2. Varela F, Lachaux JP, Rodriguez E, Martinerie J. The brainweb: phase synchronization and large-scale integration. Nat Rev Neurosci. 2001; 2:229–239. [PubMed: 11283746]
3. Schmahmann JD, Pandya DN. Cerebral white matter--historical evolution of facts and notions concerning the organization of the fiber pathways of the brain. J Hist Neurosci. 2007; 16:237–267. [PubMed: 17620190]
4. Greicius MD, Supekar K, Menon V, Dougherty RF. Resting-state functional connectivity reflects structural connectivity in the default mode network. Cereb Cortex. 2009; 19:72–78. [PubMed: 18403396]
5. Cordes D, Haughton VM, Arfanakis K, Wendt GJ, Turski PA, Moritz CH, Quigley MA, Meyerand ME. Mapping functionally related regions of brain with functional connectivity MR imaging. AJNR Am J Neuroradiol. 2000; 21:1636–1644. [PubMed: 11039342]
6. Young JP, Geyer S, Grefkes C, Amunts K, Morosan P, Zilles K, Roland PE. Regional cerebral blood flow correlations of somatosensory areas 3a, 3b, 1, and 2 in humans during rest: a PET and cytoarchitectural study. Hum Brain Mapp. 2003; 19:183–196. [PubMed: 12811734]
7. Friston KJ, Jezzard P, Turner R. Analysis of Functional MRI Time-Series. Human Brain Mapping. 1994; 1:153–171.
8. Horwitz B, Tagamets MA. Predicting human functional maps with neural net modeling. Hum Brain Mapp. 1999; 8:137–142. [PubMed: 10524605]
9. Ciccarelli O, Parker GJ, Toosy AT, Wheeler-Kingshott CA, Barker GJ, Boulby PA, Miller DH, Thompson AJ. From diffusion tractography to quantitative white matter tract measures: a reproducibility study. Neuroimage. 2003; 18:348–359. [PubMed: 12595188]
10. Matsumoto R, Nair DR, LaPresto E, Najm I, Bingaman W, Shibasaki H, Luders HO. Functional connectivity in the human language system: a cortico-cortical evoked potential study. Brain. 2004; 127:2316–2330. [PubMed: 15269116]
11. Matsumoto R, Nair DR, LaPresto E, Bingaman W, Shibasaki H, Luders HO. Functional connectivity in human cortical motor system: a cortico-cortical evoked potential study. Brain. 2007; 130:181–197. [PubMed: 17046857]
12. Umeoka S, Terada K, Baba K, Usui K, Matsuda K, Tottori T, Usui N, Nakamura F, Inoue Y, Fujiwara T, Mihara T. Neural connection between bilateral basal temporal regions: cortico-cortical evoked potential analysis in patients with temporal lobe epilepsy. Neurosurgery. 2009; 64:847–855. discussion 855. [PubMed: 19404148]
13. Matsumoto R, Kinoshita M, Taki J, Hitomi T, Mikuni N, Shibasaki H, Fukuyama H, Hashimoto N, Ikeda A. In vivo epileptogenicity of focal cortical dysplasia: a direct cortical paired stimulation study. Epilepsia. 2005; 46:1744–1749. [PubMed: 16302853]
14. Kiebel SJ, David O, Friston KJ. Dynamic causal modelling of evoked responses in EEG/MEG with lead field parameterization. Neuroimage. 2006; 30:1273–1284. [PubMed: 16490364]
15. David O, Maess B, Eckstein K, Friederici AD. Dynamic causal modeling of subcortical connectivity of language. J Neurosci. 2011; 31:2712–2717. [PubMed: 21325540]
16. Friston K. Causal modelling and brain connectivity in functional magnetic resonance imaging. PLoS Biol. 2009; 7:e33. [PubMed: 19226186]
17. Hemmelmann D, Ungureanu M, Hesse W, Wustenberg T, Reichenbach JR, Witte OW, Witte H, Leistritz L. Modelling and analysis of time-variant directed interrelations between brain regions based on BOLD-signals. Neuroimage. 2009; 45:722–737. [PubMed: 19280694]
18. Smith SM, Miller KL, Salimi-Khorshidi G, Webster M, Beckmann CF, Nichols TE, Ramsey JD, Woolrich MW. Network modelling methods for FMRI. Neuroimage. 2011; 54:875–891. [PubMed: 20817103]

19. Ferrarelli F, Haraldsson HM, Barnhart TE, Roberts AD, Oakes TR, Massimini M, Stone CK, Kalin NH, Tononi G. A [17F]-fluoromethane PET/TMS study of effective connectivity. Brain Res Bull. 2004; 64:103–113. [PubMed: 15342097]
20. Matsumoto, R.; Sawamoto, N.; Urayama, S.; Mikuni, N.; Hanakawa, T.; Behrens, T.; Ikeda, A.; Takahashi, R.; Fukuyama, H. Neuroimage. Melbourne, Austrailia: 2008. In vivo tract tracing of cortico-cortical connections in humans: a combined study of CCEP and Probabilitistic Diffusion Tractography; p. S180
21. Broca P. Remarques sur le sie`ge de la faculte' du langage articule'; suivies d'une observation d'aphemie. Bulletin de la Societe Anatomique. 1861; 2:330–357.
22. Dejerine. Anatomie Des Centres Nerveux. Paris: 1895.
23. Vandenberghe R, Price C, Wise R, Josephs O, Frackowiak RS. Functional anatomy of a common semantic system for words and pictures. Nature. 1996; 383:254–256. [PubMed: 8805700]
24. Poeppel D, Hickok G. Towards a new functional anatomy of language. Cognition. 2004; 92:1–12. [PubMed: 15037124]
25. Hickok G, Poeppel D. Dorsal and ventral streams: a framework for understanding aspects of the functional anatomy of language. Cognition. 2004; 92:67–99. [PubMed: 15037127]
26. Catani M, Jones DK, ffytche DH. Perisylvian language networks of the human brain. Ann Neurol. 2005; 57:8–16. [PubMed: 15597383]
27. Nucifora PG, Verma R, Melhem ER, Gur RE, Gur RC. Leftward asymmetry in relative fiber density of the arcuate fasciculus. Neuroreport. 2005; 16:791–794. [PubMed: 15891571]
28. Parker GJ, Luzzi S, Alexander DC, Wheeler-Kingshott CA, Ciccarelli O, Lambon Ralph MA. Lateralization of ventral and dorsal auditory-language pathways in the human brain. Neuroimage. 2005; 24:656–666. [PubMed: 15652301]
29. Basser PJ. Cable equation for a myelinated axon derived from its microstructure. Med Biol Eng Comput. 1993; 31(Suppl):S87–92. [PubMed: 8231331]
30. Haglund MM, Ojemann GA, Blasdel GG. Optical imaging of bipolar cortical stimulation. J Neurosurg. 1993; 78:785–793. [PubMed: 8468609]
31. Wada J, Rasmussen TB. Intracarotid injection of sodium amytal for the lateralization of cerebral speech dominance. J Neurosurg. 1960; 17:166–282. [PubMed: 13821345]
32. Cox RW. AFNI: software for analysis and visualization of functional magnetic resonance neuroimages. Comput Biomed Res. 1996; 29:162–173. [PubMed: 8812068]
33. Dale AM, Fischl B, Sereno MI. Cortical surface-based analysis. I. Segmentation and surface reconstruction. Neuroimage. 1999; 9:179–194. [PubMed: 9931268]
34. Fischl B, Sereno MI, Dale AM. Cortical surface-based analysis. II: Inflation, flattening, and a surface-based coordinate system. Neuroimage. 1999; 9:195–207. [PubMed: 9931269]
35. Tertel K, Tandon N, Ellmore TM. Probing brain connectivity by combined analysis of diffusion MRI tractography and electrocorticography. Comput Biol Med. 2010
36. Ellmore TM, Beauchamp MS, O'Neill TJ, Dreyer S, Tandon N. Relationships between essential cortical language sites and subcortical pathways. J Neurosurg. 2009; 111:755–766. [PubMed: 19374498]
37. Saad ZS, Ropella KM, DeYoe EA, Bandettini PA. The spatial extent of the BOLD response. Neuroimage. 2003; 19:132–144. [PubMed: 12781733]
38. Khursheed F, Tandon N, Tertel K, Pieters TA, Disano MA, Ellmore TM. Frequency-Specific Electrocorticographic Correlates of Working Memory Delay Period fMRI Activity. Neuroimage. 2011
39. Swann N, Tandon N, Canolty R, Ellmore TM, McEvoy LK, Dreyer S, DiSano M, Aron AR. Intracranial EEG reveals a time- and frequency-specific role for the right inferior frontal gyrus and primary motor cortex in stopping initiated responses. J Neurosci. 2009; 29:12675–12685. [PubMed: 19812342]
40. Fischl B, van der Kouwe A, Destrieux C, Halgren E, Segonne F, Salat DH, Busa E, Seidman LJ, Goldstein J, Kennedy D, Caviness V, Makris N, Rosen B, Dale AM. Automatically parcellating the human cerebral cortex. Cereb Cortex. 2004; 14:11–22. [PubMed: 14654453]

41. Ellmore TM, Beauchamp MS, Breier JI, Slater JD, Kalamangalam GP, O'Neill TJ, Disano MA, Tandon N. Temporal lobe white matter asymmetry and language laterality in epilepsy patients. Neuroimage. 2010; 49:2033–2044. [PubMed: 19874899]
42. Kaplan, E.; Goodglass, H.; Weintraub, S. The Boston Naming Test. Lea and Febiger; Philadelphia: 1983.
43. Lesser RP, Luders H, Klem G, Dinner DS, Morris HH, Hahn JF, Wyllie E. Extraoperative cortical functional localization in patients with epilepsy. J Clin Neurophysiol. 1987; 4:27–53. [PubMed: 3108315]
44. Tandon, N. Luders, H., editor. Cortical Mapping by Electrical Stimulation of Subdural Electrodes: Language areas.. Textbook of Epilepsy Surgery. 2008.
45. Sherbondy AJ, Dougherty RF, Napel S, Wandell BA. Identifying the human optic radiation using diffusion imaging and fiber tractography. J Vis. 2008; 8:12 11–11. [PubMed: 19146354]
46. Basser PJ, Pajevic S, Pierpaoli C, Duda J, Aldroubi A. In vivo fiber tractography using DT-MRI data. Magn Reson Med. 2000; 44:625–632. [PubMed: 11025519]
47. Tandon N, Narayana S, Lancaster JL, Brown S, Dodd S, Vollmer DG, Ingham R, Ingham J, Liotti M, Fox PT. CNS Resident Award: role of the lateral premotor cortex in articulation. Clin Neurosurg. 2003; 50:341–349. [PubMed: 14677451]
48. Glasser MF, Rilling JK. DTI tractography of the human brain's language pathways. Cereb Cortex. 2008; 18:2471–2482. [PubMed: 18281301]
49. Keller CJ, Bickel S, Entz L, Ulbert I, Milham MP, Kelly C, Mehta AD. Intrinsic functional architecture predicts electrically evoked responses in the human brain. Proc Natl Acad Sci U S A. 2011
50. Wernicke, C. Der aphasische Symptomenkomplex: eine psychologische Studie auf anatomischer Basis. Cohn & Weigert; Breslau: 1874.
51. Behrens TE, Berg HJ, Jbabdi S, Rushworth MF, Woolrich MW. Probabilistic diffusion tractography with multiple fibre orientations: What can we gain? Neuroimage. 2007; 34:144–155. [PubMed: 17070705]
52. Mori S, Wakana S, van Zijl PC, Nagae-Poetscher LM. MRI Atlas of Human White Matter. Elsevier Science.
53. Ilmoniemi RJ, Virtanen J, Ruohonen J, Karhu J, Aronen HJ, Naatanen R, Katila T. Neuronal responses to magnetic stimulation reveal cortical reactivity and connectivity. Neuroreport. 1997; 8:3537–3540. [PubMed: 9427322]
54. Matsumoto R, Nair DR, Lapresto E, Bingaman W, Shibasaki H, Luders HO. Functional connectivity in human cortical motor system: a cortico-cortical evoked potential study. Brain. 2006
55. Fox P, Ingham R, George MS, Mayberg H, Ingham J, Roby J, Martin C, Jerabek P. Imaging human intra-cerebral connectivity by PET during TMS. Neuroreport. 1997; 8:2787–2791. [PubMed: 9295118]
56. Paus T, Castro-Alamancos MA, Petrides M. Cortico-cortical connectivity of the human mid-dorsolateral frontal cortex and its modulation by repetitive transcranial magnetic stimulation. Eur J Neurosci. 2001; 14:1405–1411. [PubMed: 11703468]
57. Paus T, Jech R, Thompson CJ, Comeau R, Peters T, Evans AC. Transcranial magnetic stimulation during positron emission tomography: a new method for studying connectivity of the human cerebral cortex. J Neurosci. 1997; 17:3178–3184. [PubMed: 9096152]
58. Chouinard PA, Van Der Werf YD, Leonard G, Paus T. Modulating neural networks with transcranial magnetic stimulation applied over the dorsal premotor and primary motor cortices. J Neurophysiol. 2003; 90:1071–1083. [PubMed: 12702714]
59. Bohning DE, Shastri A, McConnell KA, Nahas Z, Lorberbaum JP, Roberts DR, Teneback C, Vincent DJ, George MS. A combined TMS/fMRI study of intensity-dependent TMS over motor cortex. Biol Psychiatry. 1999; 45:385–394. [PubMed: 10071706]
60. Fox PT, Narayana S, Tandon N, Sandoval H, Fox SP, Kochunov P, Lancaster JL. Column-based model of electric field excitation of cerebral cortex. Hum Brain Mapp. 2004; 22:1–14. [PubMed: 15083522]

61. Thielscher A, Opitz A, Windhoff M. Impact of the gyral geometry on the electric field induced by transcranial magnetic stimulation. Neuroimage. 2011; 54:234–243. [PubMed: 20682353]
62. Nathan SS, Sinha SR, Gordon B, Lesser RP, Thakor NV. Determination of current density distributions generated by electrical stimulation of the human cerebral cortex. Electroencephalogr Clin Neurophysiol. 1993; 86:183–192. [PubMed: 7680994]
63. Crick F, Jones E. Backwardness of human neuroanatomy. Nature. 1993; 361:109–110. [PubMed: 8421513]
64. DeFelipe J. From the connectome to the synaptome: an epic love story. Science. 330:1198–1201. [PubMed: 21109663]
65. McKeown MJ, Makeig S, Brown GG, Jung TP, Kindermann SS, Bell AJ, Sejnowski TJ. Analysis of fMRI data by blind separation into independent spatial components. Hum Brain Mapp. 1998; 6:160–188. [PubMed: 9673671]
66. Smith SM, Fox PT, Miller KL, Glahn DC, Fox PM, Mackay CE, Filippini N, Watkins KE, Toro R, Laird AR, Beckmann CF. Correspondence of the brain's functional architecture during activation and rest. Proc Natl Acad Sci U S A. 2009; 106:13040–13045. [PubMed: 19620724]
67. Robinson JL, Laird AR, Glahn DC, Lovallo WR, Fox PT. Metaanalytic connectivity modeling: delineating the functional connectivity of the human amygdala. Hum Brain Mapp. 2010; 31:173–184. [PubMed: 19603407]
68. Laird AR, Eickhoff SB, Kurth F, Fox PM, Uecker AM, Turner JA, Robinson JL, Lancaster JL, Fox PT. ALE Meta-Analysis Workflows Via the Brainmap Database: Progress Towards A Probabilistic Functional Brain Atlas. Front Neuroinform. 2009; 3:23. [PubMed: 19636392]
69. Le Bihan D. Looking into the functional architecture of the brain with diffusion MRI. Nat Rev Neurosci. 2003; 4:469–480. [PubMed: 12778119]
70. Behrens TE, Johansen-Berg H. Relating connectional architecture to grey matter function using diffusion imaging. Philos Trans R Soc Lond B Biol Sci. 2005; 360:903–911. [PubMed: 16087435]
71. Mori S, Zhang J. Principles of diffusion tensor imaging and its applications to basic neuroscience research. Neuron. 2006; 51:527–539. [PubMed: 16950152]
72. Laird AR, Fox PM, Eickhoff SB, Turner JA, Ray KL, McKay DR, Glahn DC, Beckmann CF, Smith SM, Fox PT. Behavioral Interpretations of Intrinsic Connectivity Networks. J Cogn Neurosci. 2011
73. Song SK, Sun SW, Ju WK, Lin SJ, Cross AH, Neufeld AH. Diffusion tensor imaging detects and differentiates axon and myelin degeneration in mouse optic nerve after retinal ischemia. Neuroimage. 2003; 20:1714–1722. [PubMed: 14642481]
74. Song SK, Sun SW, Ramsbottom MJ, Chang C, Russell J, Cross AH. Dysmyelination revealed through MRI as increased radial (but unchanged axial) diffusion of water. Neuroimage. 2002; 17:1429–1436. [PubMed: 12414282]
75. Behrens TE, Johansen-Berg H, Woolrich MW, Smith SM, Wheeler-Kingshott CA, Boulby PA, Barker GJ, Sillery EL, Sheehan K, Ciccarelli O, Thompson AJ, Brady JM, Matthews PM. Non-invasive mapping of connections between human thalamus and cortex using diffusion imaging. Nat Neurosci. 2003; 6:750–757. [PubMed: 12808459]

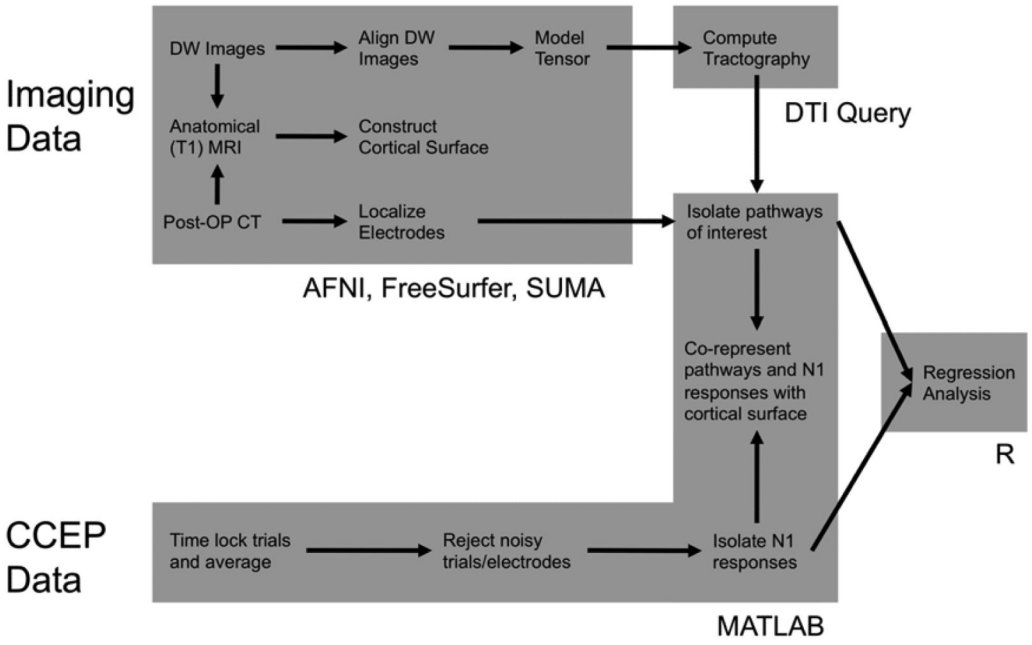


**Figure 1.**

Data processing flow chart for CCEP response-tractography correlation. Two separate processing streams (Imaging and Electrophysiology) were carried out independently using dedicated software. Localization of SDEs in imaging space allowed for inter-modality comparison by joining the two datasets in a common frame of reference. Selection of pathways, processing of electrophysiology and co-representation of data (Figure 3) were all performed in Matlab using in house software. Pathway numbers and N1 responses were exported into R for the final regression (Figure 4) analysis with all subjects and stimulating pairs were pooled together.

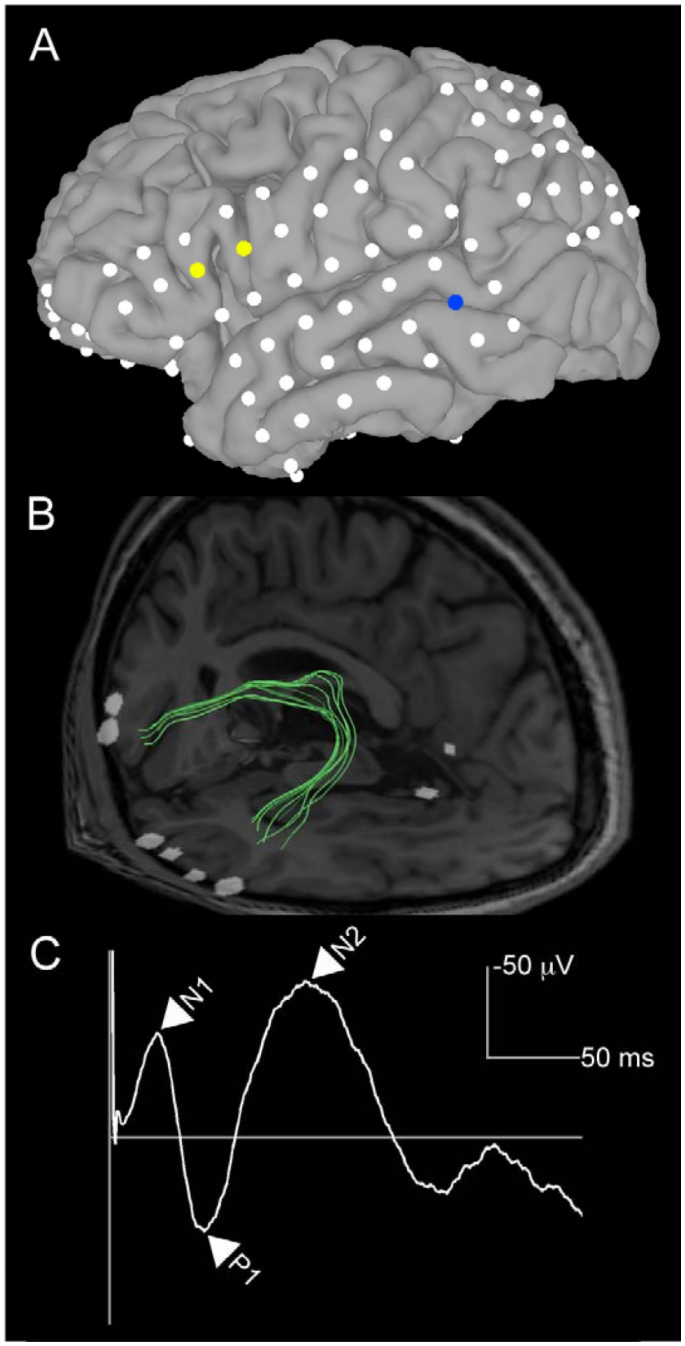


**Figure 2.**

Anterior to posterior CCEP response. (A) Electrodes represented on the cortical surface in FreeSurfer. Stimulating pair of electrodes displayed in yellow overlaying BA in both PT and PO and with the posterior, recording electrode in Wernicke's shown in blue. (B) DTI tractography between the stimulating and recording electrode pair. Pathways were selected using cuboidal VOIs 20 mm on a side. Pathways were constrained to pass from either stimulating electrode to the recording electrode. (C) Prominent N1 response of the blue electrode (latency = 31 ms, amplitude = 48.8 mV) recorded at Wernicke's electrode during stimulation of BA (yellow electrodes).

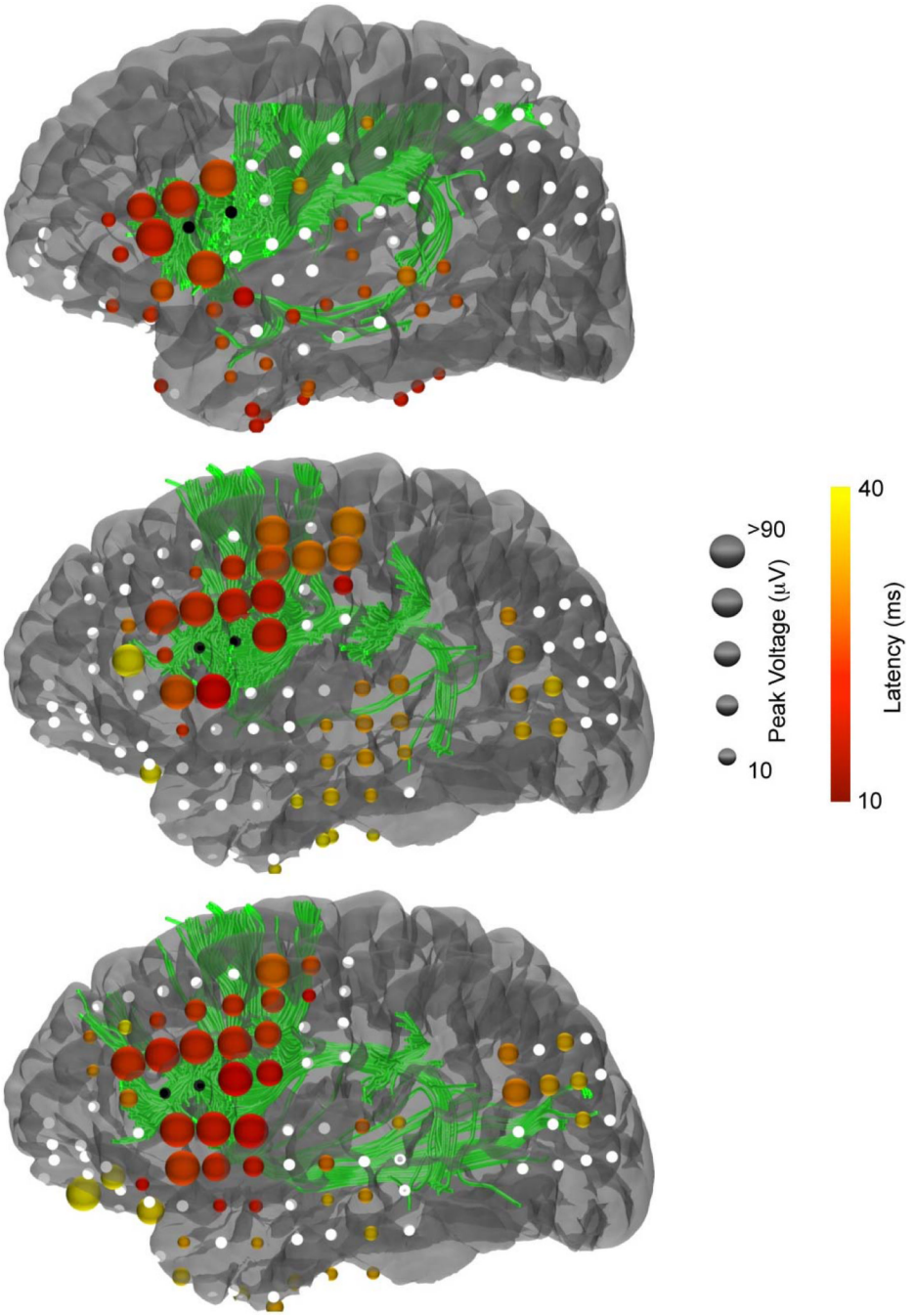


**Figure 3.**

Co-representation of DTI pathways and CCEPs from stimulation of anterior language site. Two illustrative subjects CCEP responses during stimulation of BA. The top row represents one subject (no. 7, stimulation pair no. 10) while middle and bottom row are two separate stimulation pairs in the same subject (no. 5, stimulation pairs 7 and 8). Black electrodes denote the stimulating pair of electrodes. Subsequent N1 response measured at all other electrodes represented in terms of amplitude (radius of electrode) and latency (color). Electrodes without CCEP response are depicted as white spheres. All pathways passing through 20mm cubes centered at the stimulating pair are shown as green streamlines. The top row contains the same stimulating pair and response as in Figure 2.

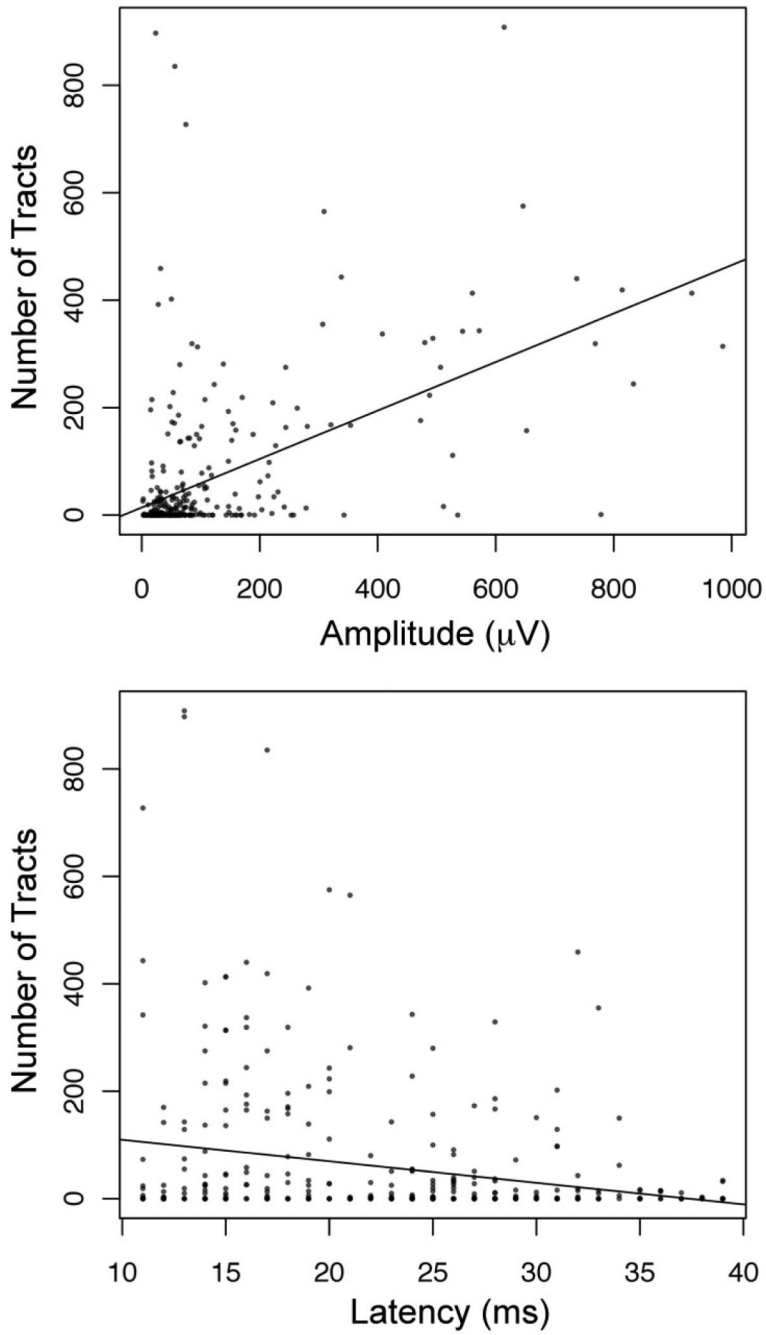


**Figure 4.**

Regression results of number of pathways between stimulating pair and each electrode vs N1 response. All patients and stimulation pairs were pooled together for one analysis. A total of 408 electrodes had N1 responses following anterior language site stimulation (those without N1 response are excluded from the analysis). Regression between amplitude and latency demonstrated a positive and negative relationship, respectively, with strength of path between the stimulation pair and the recording electrodes.

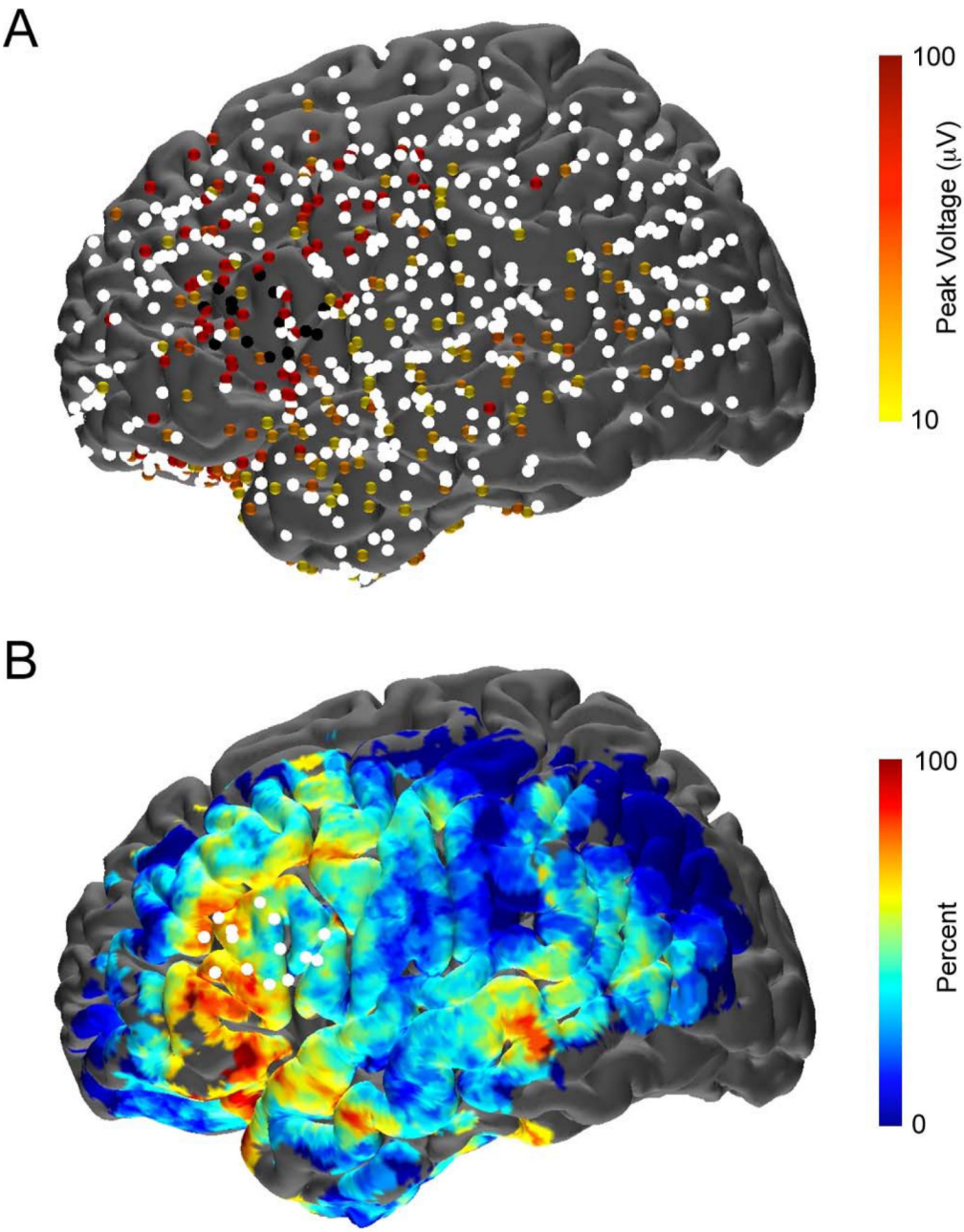


**Figure 5.**

Grouped representation of N1 responses. (A) Representation of the N1 responses of the CCEP for the group (n = 7) across 837 electrodes following stimulation at 10 distinct electrodes pairs located over BA. N1 responses at each electrode were color coded by amplitude as shown in the legend. Electrodes in white had either no CCEP response or one with an amplitude of < 10 μV. (B) Distribution of N1 responses across all patients. Each point on the cortical surface was colored based on the number of electrodes within 7 mm that had an N1 response. Only locations with >2 electrodes nearby were included to avoid outliers caused by sparse sampling. The white electrodes represent stimulating electrodes.

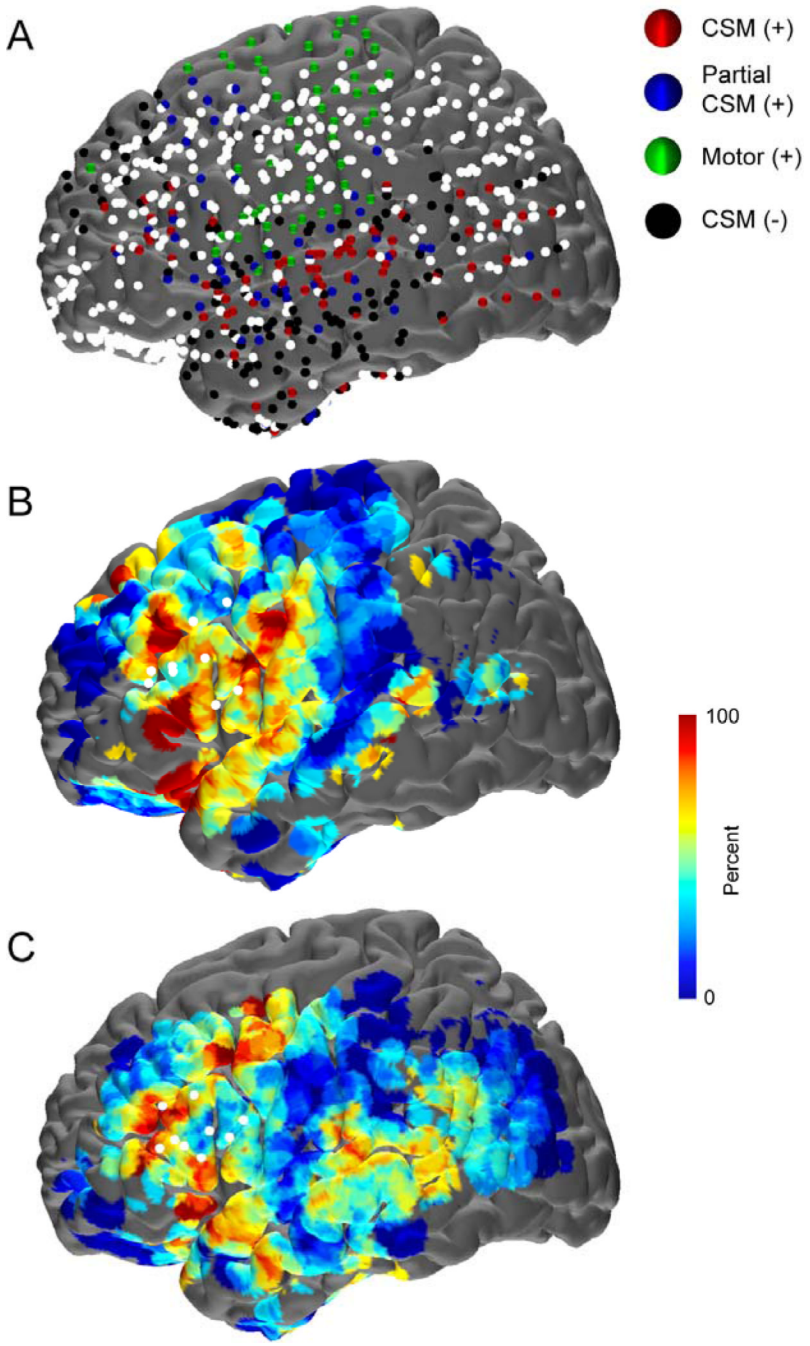


**Figure 6.**

Results of cortical stimulation mapping (CSM) and N1 responses grouped by CSM positive and negative pairs. (A) CSM results categorized for all SDEs implanted. Electrodes which consistently caused a deficit during stimulation are shown in red, those which caused a deficit when part of one stimulating pair, but not another (edge effects) are in blue, SDEs which only resulted in a motor effect are green, those that were stimulated but never caused a deficit are black and all SDEs which were not evaluated by CSM are white. (B) Representation of the N1 responses during CCEP stimulation at electrode pairs that were CSM positive (no. 2-6). (C) Distribution of N1 responses across CCEP stimulation pairs, which were negative (no. 7-9) or not tested (no. 1 and 10). Only those brain surface

locations with >2 electrodes within 8 mm were included to avoid distortion of the results by outliers.

**Table 1**

**Patient Demographics**

Subject demographics and electrode numbers. In two subjects (no. 4, 5), multiple pairs of electrodes were located over BA and were stimulated with CCEPs individually. Anatomical location of each stimulating pair was classified, and in only one case (no. 10) did the location of the two electrodes differ. The CSM results and maximum current level for each pair were categorized. CSM deficits were classified as positive in the case of speech arrest, auditory repetition (AR), auditory naming (AN) and visual naming (VN). If CSM did not produce a language deficit then that pair was labeled a negative (Neg) language site. Two pairs (no. 1, 10) did not have CSM mapping performed and were unclassified.

| PT | Age | Sex | IQ | Wada Result | Number of Electrodes | Stimulation Pair # | Locus | CSM Result | Max Current (mA) |
|---|---|---|---|---|---|---|---|---|---|
| 1 | 61 | F | 100 | N/A | 107 | 1 | PT | - | - |
| 2 | 37 | F | 89 | Left | 108 | 2 | PO | Speech Arrest | 8 |
| 3 | 39 | M | 100 | N/A | 117 | 3 | PT | AR/AN/VN | 10 |
| 4 | 17 | M | 67 | Left | 142 | 4 | PT | AN/VN | 8 |
| | | | | | | 5 | PT | AN | 7 |
| | | | | | | 6 | PO | AR | 8 |
| 5 | 30 | F | 100 | Left | 127 | 7 | PT | Neg | 8 |
| | | | | | | 8 | PO | Neg | 6 |
| 6 | 42 | F | 107 | Left | 127 | 9 | Both | Neg | 8 |
| 7 | 28 | F | 97 | Left | 109 | 10 | PT | - | - |